ChemComm

Chemical Communications

rsc.li/chemcomm

ROYAL SOCIETY
OF CHEMISTRY
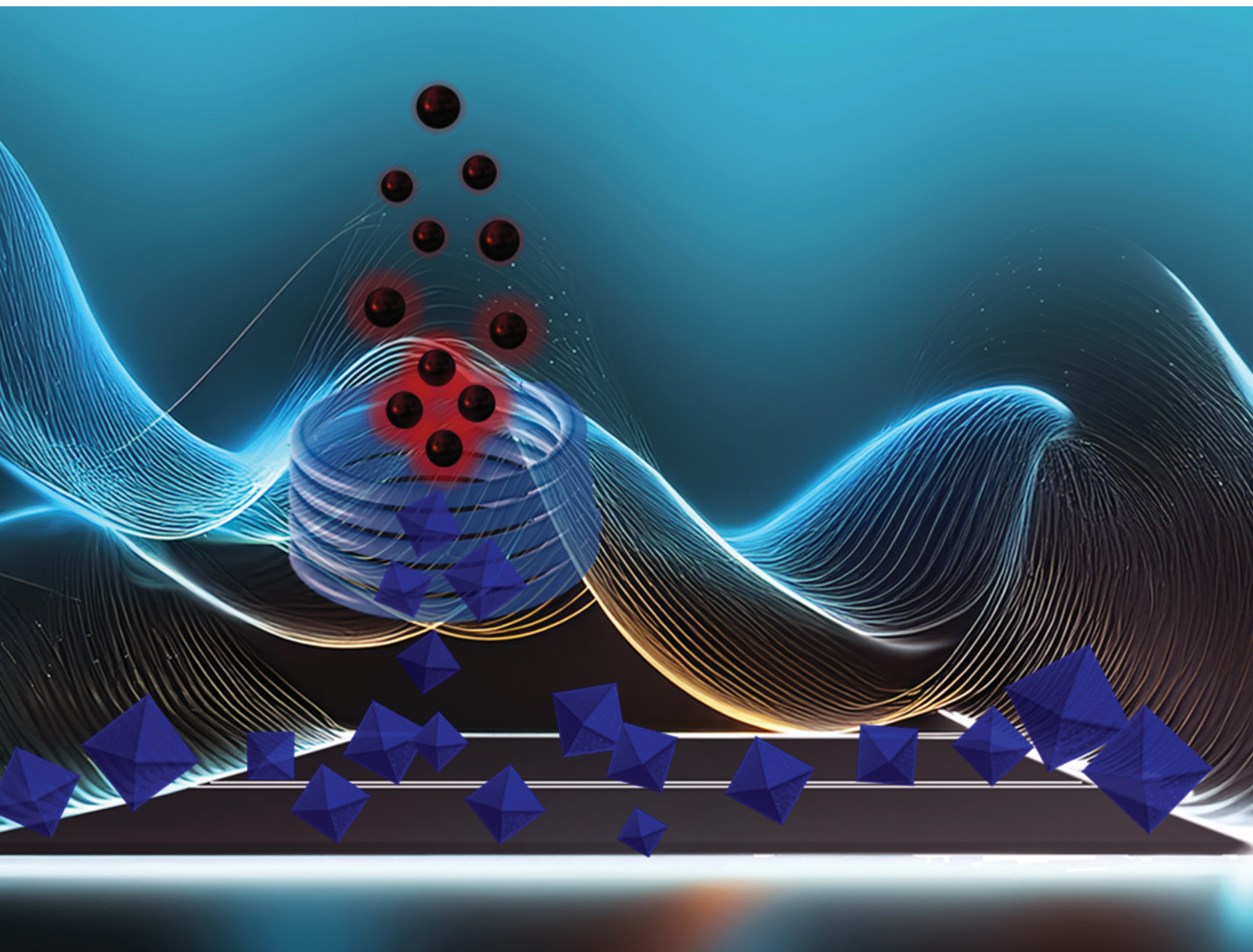
COMMUNICATION
Gaurav Verma, Shengqian Ma *et al.*
Magnetically induced localized heating enabling rapid and
efficient synthesis of metal–organic frameworks

Check for updates

Magnetically induced localized heating enabling rapid and efficient synthesis of metal–organic frameworks†

Mansi Kapoor,[a] Saikumar Dussa,[b] Narendra B. Dahotre,[c] Gaurav Verma*[a] and Shengqian Ma [ID] *[a]

We demonstrate magnetic induction heating (MIH) with superparamagnetic iron oxide nanoparticles (IONPs) as a new rapid and energy-efficient methodology for synthesizing metal–organic frameworks (MOFs). Acting as localized heat sources, these IONPs overcome the energy losses associated with traditional solvothermal synthesis, which enables a fast, uniform, and highly energy-efficient heat transfer process. The versatility of this method is illustrated for the successful synthesis of three different benchmark MOFs in good yields with high crystallinity.

Over the past couple of decades, metal–organic frameworks (MOFs) have established themselves as a leading class of materials in the realm of porous materials research.[1] Comprised of metal nodes or secondary building units (SBUs) connected by organic ligands to form periodic networks, MOFs boast high crystallinity, adjustable pore sizes and geometries, structural diversity, ultrahigh surface areas, and accessible binding sites.[2] These versatile materials have found applications in numerous fields,[3] including gas storage and separation,[4] catalysis,[5] sensing,[6] drug delivery,[7] optoelectronics,[8] and energy storage.[9] Recently, efforts to scale up and commercialize these materials have gained momentum, leading to the emergence of various industries and start-ups utilizing them.[10–13] To optimize the production costs, there has been a strong emphasis on developing efficient synthesis techniques to foster the widespread deployment of these materials.

Solvothermal synthesis is the most conventional and widely used method for obtaining MOFs, but it has significant drawbacks, including lengthy reaction times, high energy consumption, safety risks, and scalability issues.[14] Recent advancements in synthetic methodologies have introduced alternative routes

such as mechanochemical, electrochemical, sonochemical, continuous flow, microwave-assisted, and photothermal synthesis, which offer notable benefits.[12,15–21] Despite these advancements, challenges related to yield, product crystallinity, universality, penetration depth, and energy losses still persist.[14] Therefore, there is a continuous need to explore and develop alternative efficient and effective MOF synthesis techniques.

Induction heating is a convenient, contactless, fast, safe, and precise method, offering advantages over classical heating methods based on convection and radiation.[22] Hereby, heat is generated on the surface of the workpiece placed within a changing magnetic field. These unparalleled features have made induction heating suitable for numerous applications, including biomedical drug release, metallurgical manufacturing of metals and alloys, catalytic processes, and driving chemical reactions.[22–24] Specifically, magnetic induction heating (MIH) of iron oxide nanoparticles (IONPs) is a promising technology that has recently been employed in materials science and medical therapy.[25–27] This process involves applying an alternating magnetic field to these nanoparticles, causing them to rapidly generate heat. This occurs through relaxation losses: specifically Néel and Brownian relaxation in the superparamagnetic regime, allowing the nanoparticles to serve as localized heat sources.[28–30] This capability has been leveraged for obtaining magnetic framework composite materials (MFCs) that have been utilized in hyperthermia therapy and explored for stimuli-triggered release of guest molecules.[31–33] Hill and Li *et al.* utilized the induction heating for the preparation and regeneration of MFCs;[34–37] and very recently we demonstrated the confinement of IONPs in MOF as carriers for magnetothermally-triggered drug release (MTDR).[38] However, despite its promising potential, the utilization of the magnetic induction heating as a synthetic technique for producing pure-phase MOFs is still unprecedented.

In this work, we report the rapid and efficient synthesis of MOFs induced by localized magnetic induction heating of superparamagnetic iron oxide nanoparticles. Three different

[a] *Department of Chemistry, University of North Texas, 1508 W Mulberry St., Denton, TX, 76201, USA. E-mail: Shengqian.Ma@unt.edu, Gaurav.Verma@unt.edu*
[b] *Center for Agile and Adaptive Additive Manufacturing, University of North Texas, 3940 N Elm St, Denton, TX 76207, USA*
[c] *Department of Materials Science and Engineering, University of North Texas, 3940 N Elm St, Denton, TX 76207, USA*

types of MOFs (HKUST-1,[39] MOF-235,[40] and MOF-5[41]) were synthesized using different solvent systems and achieved in good yields over a significantly reduced time period, demonstrating the efficacy and versatility of this methodology. The resulting MOFs could be easily extracted *via* magnetic separation, and the IONP system was evaluated for reutilization in subsequent syntheses.

The iron oxide nanoparticles were synthesized *via* co-precipitation,[42] followed by surface modification with polyethylene glycol (PEG) to produce monodisperse **PEG-1000@IONPs** with an average hydrodynamic diameter of 140 nm (Fig. S1, ESI†). The surface coating with PEG is crucial for enhancing the stability of the IONPs, preventing agglomeration and oxidation. Moreover, the use of coatings featuring carboxylic acid groups usually leads to the formation of composites.[35,36,38] Thus, judicious selection of PEG as the coating was essential to prevent the composite formation and enable ease of separation. The metal–oxygen (Fe–O) characteristic vibration band was observed at approximately 537 cm^{-1}, and the presence of PEG was confirmed by the characteristic –CH$_2$, –CH, and C–O–C bond stretching vibrations at around 2922, 1416, and 1060 cm^{-1}, respectively (Fig. S2, ESI†).[42] Additionally, a shift in the –OH stretching vibration indicated interaction between the PEG and IONPs. The crystalline structure of the **PEG-1000@IONPs** matched well with the cubic inverse spinel structure of magnetite reported in the literature, as indicated by the diffraction peaks corresponding to the (220), (311), (400), (511), and (440) planes in the PXRD pattern (Fig. 1a).[42] The superparamagnetic nature of the material[42–44] was confirmed through magnetic property measurements, with the magnetization *vs.* magnetic field (*M–H*) curves at room temperature showing negligible hysteresis, nearly zero remanence, and an intrinsic coercivity of ∼7 Oe. Additionally, a high saturation magnetization value of 70 emu g^{-1} at an applied magnetic field of 30 kOe was observed for the **PEG-1000@IONPs**, as shown in Fig. 1b.

Next, we aimed to evaluate the heating efficacy of super-paramagnetic PEG-coated iron oxide nanoparticles under a magnetic field and explore the potential of utilizing magnetic induction heating for MOF synthesis. We began by investigating the synthesis of HKUST-1, an early and well-known example of MOFs known for its high surface area and porosity. HKUST-1 has been extensively studied for various applications, including

gas storage and separation, sensing, drug delivery, electrocatalysis, and biomedicine.[45] The traditional solvothermal synthesis of HKUST-1 was first reported by Chui *et al.* in 1999,[39] involving an EtOH/water solvent system at 180 °C. However, these conditions were not feasible for our system (see Fig. S3, ESI† for the detailed experimental setup) as the synthesis must be carried out at ambient pressure, and such high temperature would lead to solvent evaporation. Therefore, we adapted the solvothermal synthesis method reported by Laszlo *et al.*[46] which is conducted at 80 °C. Firstly, we examined the heating properties of these nanoparticles within the EtOH/water solvent system. Varying concentrations of **PEG-1000@IONPs** (2.5 mg mL^{-1}, 5 mg mL^{-1}, and 7.5 mg mL^{-1}) were each dispersed in 5 mL of a 1:1 EtOH:water mixture and exposed to an alternating magnetic field of 35.32 kA m^{-1} (frequency: 224 kHz) for 30 minutes. A rapid temperature increase was observed, stabilizing at ∼58 °C for the 2.5 mg mL^{-1} dispersion and ∼69 °C for the 5 mg mL^{-1} dispersion. However, for the 7.5 mg mL^{-1} dispersion, the solvent began bubbling upon reaching 81 °C due to the temperature nearing solvents' boiling point, resulting in significant temperature fluctuations (Fig. S4a, ESI†). Therefore, the 5 mg mL^{-1} concentration of **PEG-1000@IONPs** was selected as the optimal concentration for utilization in this MOF synthesis. The effect of magnetic field strength was also determined, showing a gradual temperature increase with higher field strengths (Fig. S4b, ESI†). Based on these optimized conditions, 5 mg mL^{-1} of **PEG-1000@IONPs** were dispersed in 5 mL of HKUST-1 precursor solution and subjected to an alternating magnetic field of 35.32 kA m^{-1} at 224 kHz (Fig. 2a). The temperature rapidly rose, stabilizing around 65 °C (±1 °C) within 15 minutes (Fig. 2b). Remarkably, MOF formation was observed after just 20 minutes. The resultant material (**HKUST-1 MIH-20min**) was isolated *via* magnetic separation, and analyzed using PXRD and scanning electron microscopy (SEM). The analyses confirmed the presence of pure HKUST-1 phase, consistent with the calculated PXRD pattern (Fig. 3a), and SEM images revealed the formation of tiny octahedrons characteristic of HKUST-1 crystals[39] (Fig. 3b). The reaction was monitored over time, with products extracted and isolated at the intervals of 20 min (**HKUST-1 MIH-20min**), 40 min (**HKUST-1 MIH-40min**),
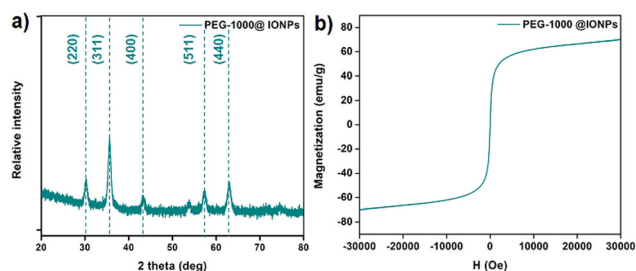

Fig. 1 (a) PXRD pattern indicating phase purity, and (b) magnetization curve showing negligible hysteresis for **PEG-1000@IONPs**.
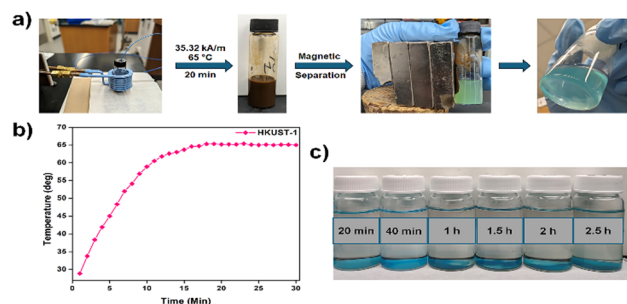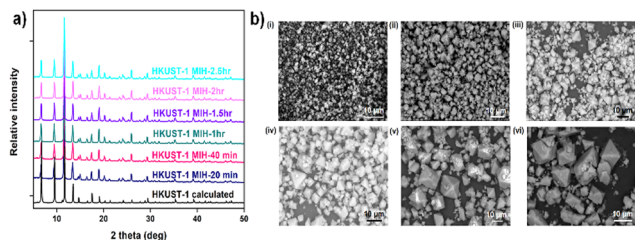

Fig. 2 (a) The schematic of the MIH synthesis for HKUST-1 carried out at 60 °C for 20 min, followed by magnetic separation to yield pure MOF, (b) heating profile of the **PEG-1000@IONPs**, and (c) the products obtained at different time intervals extracted using the same procedure as shown in (a).

Fig. 3 Characterization of the HKUST-1 products obtained at different time intervals: (a) the PXRD patterns compared to the calculated pattern of HKUST-1, and (b) SEM images of (i) **HKUST-1 MIH-20min**, (ii) **HKUST-1 MIH-40min**, (iii) **HKUST-1 MIH-1h**, (iv) **HKUST-1 MIH-1.5h**, (v) **HKUST-1 MIH-2h**, and (vi) **HKUST-1 MIH-2.5h**.

60 min (**HKUST-1 MIH-1h**), 90 min (**HKUST-1 MIH-1.5h**), 120 min (**HKUST-1 MIH-2h**), and 150 min (**HKUST-1 MIH-2.5h**). The obtained products are shown in Fig. 2c. The yield increased progressively, from 6.6% at 20 min to 41.5% at 2.5 h (Fig. S5, ESI†). In contrast, the solvothermal synthesis conducted in a convection oven at 65 °C for 2.5 h (**HKUST-1 ST-2.5h**) resulted in a crystalline phase (Fig. S6, ESI†) of only 11.7% yield, with no discernible phase formation observed after 20 minutes.

This significant reduction in reaction time with increased yields can be attributed to the localized MIH generated by the nanoparticles acting as nanoheaters, which accelerates the reaction and enhances the energy efficiency of the synthesis process. The PXRD patterns of all the products obtained from MIH heating were identical to the calculated pattern of HKUST-1 (Fig. 3a), indicating high crystallinity and phase purity. Additionally, the growth of the crystals during the synthesis was evident from SEM micrographs, which showed a gradual increase in the size of the HKUST-1 octahedrons (Fig. 3b), reaching an average size of 11.61 μm × 8.37 μm for **HKUST-1 MIH-2.5h.**

To evaluate the porosity of **HKUST-1 MIH-2.5h**, Brunauer–Emmett–Teller (BET) surface area measurements were conducted using N_2 adsorption–desorption isotherms on the material activated at 120 °C under dynamic vacuum. The measurements revealed a total N_2 uptake of approximately 388 cm^3 g^{-1} and a high BET surface area of 1115 m^2 g^{-1} (Fig. S7, ESI†), comparable to the values reported for conventional solvothermal synthesis by Laszlo et al.[46] The **HKUST-1 ST-2.5h** on the other hand displayed negligible porosity, indicating the formation of a crystalline non-porous phase after 2.5 h of the conventional solvothermal synthesis and the necessity for the longer reaction time. It is thus noteworthy that the MIH synthesis produced a product with similar quality in terms of crystallinity and porosity, but at a lower reaction temperature and significantly reduced reaction time compared to the traditional solvothermal method. Additionally, the power consumption for MIH synthesis was only 191 W, which is significantly less than the power required for convection ovens used in traditional solvothermal synthesis. These ovens not only consume more power but also suffer from longer heat-up times and power losses due to heat dissipation to the environment (Table S1, ESI†).

The stability and activity of the **PEG-1000@IONPs** after the synthesis were also evaluated. Following the extraction of the pure MOF, the IONPs were washed with ethanol multiple times and then dried. The material exhibited remarkable stability with negligible loss in crystallinity, as indicated by the PXRD pattern (Fig. S8a, ESI†). The IONPs were then redispersed in the HKUST-1 precursor solution. Upon reapplying the same magnetic field strength, the system again quickly reached a temperature of 66 °C within 15 minutes (Fig. S8b, ESI†) and maintained this temperature throughout the 2.5-hour reaction, demonstrating the excellent reusability of the IONP system. The **HKUST-1 MIH-2.5h** product was obtained again with a high yield of 43.1%, attributed to the slightly higher temperature during this run. Thus, the high efficacy and efficiency of the MIH synthesis using **PEG-1000@IONPs** were established.

To further evaluate the scope and versatility of the MIH synthesis, we applied it to synthesize two additional MOFs: MOF-235 and MOF-5. The synthesis of MOF-235 is particularly challenging due to the potential formation of the MIL-101 phase, which depends on the ratio of metal-to-linker and the solvents used. Simonsson et al.[47] reported the phase-pure synthesis of MOF-235 using a stoichiometric ratio of Fe(III) to terephthalic acid (4:3) in a 3:1 DMF:EtOH system at 80 °C. For our MIH synthesis, we followed a similar procedure with slight modifications. **PEG1000@IONPs** at a concentration of 5 mg mL^{-1} were dispersed in the MOF-235 precursor solution, rapidly reaching 85 °C within 10 minutes (Fig. S9, ESI†) under a magnetic field strength of 31.23 kA m^{-1} (224 kHz frequency). Notably, the system required less power to achieve this temperature in the DMF/EtOH system due to the different heating behavior of the **PEG-1000@IONPs** in various solvent systems. After 2.5 hours, MOF-235 was obtained in good yield and high phase purity, as confirmed by the PXRD pattern, which matched well with the calculated pattern (Fig. S10b, ESI†). SEM images also revealed well-crystallized octahedral structures of MOF-235 (average size 3.59 μm × 1.43 μm) as shown in Fig. S10a (ESI†), consistent with literature reports.[47]

For MOF-5, we modified the solvothermal synthesis procedure described by Chen et al.,[48] which is typically conducted at 120 °C. To achieve a higher synthesis temperature, we used a higher concentration of **PEG-1000@IONPs** (7.5 mg mL^{-1}) dispersed in the MOF-5 mother liquor with DMF as the solvent. The application of a magnetic field strength of 60.92 kA m^{-1} (at 224 kHz) led to a rapid temperature increase, stabilizing around 98 °C after 15 min (Fig. S11, ESI†). The reaction was conducted for 2.5 hours, resulting in phase-pure MOF-5 (Fig. S12b, ESI†) with a good yield at a significantly lower reaction temperature. SEM imaging revealed cubic MOF-5 crystals with an average size of 10.50 μm (Fig. S12a, ESI†), confirming the high crystallinity of the product. Thus, the MIH methodology's general applicability for the synthesis of MOFs was successfully demonstrated.

In conclusion, we demonstrated the use of magnetic induction heating with superparamagnetic iron oxide nanoparticles as a new methodology for synthesizing MOFs. The localized heating generated by the IONPs acting as nanoheaters

addresses the energy losses typically encountered in conventional solvothermal synthesis, offering a rapid, uniform, and highly energy-efficient heat transfer process. Using MIH, we successfully synthesized three benchmark MOF materials (HKUST-1, MOF-5, and MOF-235) across different reaction systems and synthesis temperatures, achieving good yields and high crystallinity. Additionally, the IONPs could be easily separated from the reaction system post-synthesis and reused without any loss of activity, further enhancing the synthesis efficacy. Furthermore, the IONPs were easily separable from the reaction system post-synthesis and could be reused without any loss in activity, enhancing the overall efficacy of the synthesis. Therefore, MIH synthesis presents itself as a promising alternative approach with significant potential for the effective and efficient synthesis of MOFs. We plan to continue developing the MIH synthesis methodology and explore various IONP systems to improve yields and efficiency, extending its application to the synthesis of various other MOFs.

Data availability

The data supporting this article have been included as part of the ESI.†

Conflicts of interest

There are no conflicts to declare.

Notes and references

1 J. E. Mondloch, R. C. Klet, A. J. Howarth, J. T. Hupp and O. K. Farha, *Handbook of Solid State Chemistry*, 2017, pp. 165–193, DOI: 10.1002/9783527691036.hsscvol4016.
2 H.-C. Zhou, J.-R. Long and O. M. Yaghi, *Chem. Rev.*, 2012, **112**, 673–674.
3 S. Ma and J. A. Perman, *Elaboration and Applications of Metal-Organic Frameworks*, World Scientific, 2017.
4 C. Jiang, X. Wang, Y. Ouyang, K. Lu, W. Jiang, H. Xu, X. Wei, Z. Wang, F. Dai and D. Sun, *Nanoscale Adv.*, 2022, **4**, 2077–2089.
5 V. Pascanu, G. González Miera, A. K. Inge and B. Martín-Matute, *J. Am. Chem. Soc.*, 2019, **141**, 7223–7234.
6 J. F. Olorunyomi, S. T. Geh, R. A. Caruso and C. M. Doherty, *Mater. Horiz.*, 2021, **8**, 2387–2419.
7 H. D. Lawson, S. P. Walton and C. Chan, *ACS Appl. Mater. Interfaces*, 2021, **13**, 7004–7020.
8 K. Zhou, Y. Zhou, Z. Jia, G. Ding, X.-Q. Ma, W. Niu, S. Yang, S.-T. Han, J. Zhao and Y. Zhou, *Cell Rep. Phys. Sci.*, 2023, **4**, 101656.
9 T. Qiu, Z. Liang, W. Guo, H. Tabassum, S. Gao and R. Zou, *ACS Energy Lett.*, 2020, **5**, 520–532.
10 Q. He, F. Zhan, H. Wang, W. Xu, H. Wang and L. Chen, *Mater. Today Sustain.*, 2022, **17**, 100104.
11 A. U. Czaja, N. Trukhan and U. Müller, *Chem. Soc. Rev.*, 2009, **38**, 1284–1293.
12 D. Chakraborty, A. Yurdusen, G. Mouchaham, F. Nouar and C. Serre, *Adv. Funct. Mater.*, 2023, 2309089.
13 E. Wang, R. Navik, Y. Miao, Q. Gao, D. Izikowitz, L. Chen and J. Li, *Cell Rep. Phys. Sci.*, 2024, **5**, 101791.
14 Y. Li, G. Wen, J. Li, Q. Li, H. Zhang, B. Tao and J. Zhang, *Chem. Commun.*, 2022, **58**, 11488–11506.
15 D. Li, A. Yadav, H. Zhou, K. Roy, P. Thanasekaran and C. Lee, *Global Challenges*, 2024, **8**, 2300244.
16 K. A. S. Usman, J. W. Maina, S. Seyedin, M. T. Conato, L. M. Payawan, L. F. Dumée and J. M. Razal, *NPG Asia Mater.*, 2020, **12**, 58.
17 H. Ren and T. Wei, *ChemElectroChem*, 2022, **9**, e202200196.
18 C. Vaitsis, G. Sourkouni and C. Argirusis, *Ultrason. Sonochem.*, 2019, **52**, 106–119.
19 P. A. Bayliss, I. A. Ibarra, E. Pérez, S. Yang, C. C. Tang, M. Poliakoff and M. Schröder, *Green Chem.*, 2014, **16**, 3796–3802.
20 I. Thomas-Hillman, A. Laybourn, C. Dodds and S. W. Kingman, *J. Mater. Chem. A*, 2018, **6**, 11564–11581.
21 O. Shelonchik, N. Lemcoff, R. Shimoni, A. Biswas, E. Yehezkel, D. Yesodi, I. Hod and Y. Weizmann, *Nat. Commun.*, 2024, **15**, 1154.
22 O. Lucía, P. Maussion, E. J. Dede and J. M. Burdío, *IEEE Trans. Ind. Electron*, 2014, **61**, 2509–2520.
23 W. Wang, G. Tuci, C. Duong-Viet, Y. Liu, A. Rossin, L. Luconi, J.-M. Nhut, L. Nguyen-Dinh, C. Pham-Huu and G. Giambastiani, *ACS Catal.*, 2019, **9**, 7921–7935.
24 C. Kuhwald, S. Türkhan and A. Kirschning, *Beilstein J. Org. Chem.*, 2022, **18**, 688–706.
25 S. R. Yassine, Z. Fatfat, G. H. Darwish and P. Karam, *Catal. Sci. Technol.*, 2020, **10**, 3890–3896.
26 M. I. Anik, M. K. Hossain, I. Hossain, A. M. U. B. Mahfuz, M. T. Rahman and I. Ahmed, *Nano Select*, 2021, **2**, 1146–1186.
27 T. Raczka, A. Wolf, J. Reichstein, C. Stauch, B. Schug, S. Müssig and K. Mandel, *J. Magn. Magn. Mater.*, 2024, **598**, 172042.
28 Z. Ma, J. Mohapatra, K. Wei, J. P. Liu and S. Sun, *Chem. Rev.*, 2023, **123**, 3904–3943.
29 J. Mohapatra, M. Xing and J. P. Liu, *Materials*, 2019, **12**, 3208.
30 J. Mohapatra, F. Zeng, K. Elkins, M. Xing, M. Ghimire, S. Yoon, S. R. Mishra and J. P. Liu, *Phys. Chem. Chem. Phys.*, 2018, **20**, 12879–12887.
31 X. Ge, R. Wong, A. Anisa and S. Ma, *Biomaterials*, 2022, **281**, 121322.
32 H. Gavilán, S. K. Avugadda, T. Fernández-Cabada, N. Soni, M. Cassani, B. T. Mai, R. Chantrell and T. Pellegrino, *Chem. Soc. Rev.*, 2021, **50**, 11614–11667.
33 M. M. Sadiq, H. Li, A. J. Hill, P. Falcaro, M. R. Hill and K. Suzuki, *Chem. Mater.*, 2016, **28**, 6219–6226.
34 H. Li, M. M. Sadiq, K. Suzuki, R. Ricco, C. Doblin, A. J. Hill, S. Lim, P. Falcaro and M. R. Hill, *Adv. Mater.*, 2016, **28**, 1839–1844.
35 H. Li, M. M. Sadiq, K. Suzuki, P. Falcaro, A. J. Hill and M. R. Hill, *Chem. Mater.*, 2017, **29**, 6186–6190.
36 Y. Tao, G. Huang, H. Li and M. R. Hill, *ACS Sustainable Chem. Eng.*, 2019, **7**, 13627–13632.
37 H. Li, M. M. Sadiq, K. Suzuki, C. Doblin, S. Lim, P. Falcaro, A. J. Hill and M. R. Hill, *J. Mater. Chem.*, 2016, **4**, 18757–18762.
38 X. Ge, J. Mohapatra, E. Silva, G. He, L. Gong, T. Lyu, R. P. Madhogaria, X. Zhao, Y. Cheng, A. M. Al-Enizi, A. Nafady, J. Tian, J. P. Liu, M.-H. Phan, F. Taraballi, R. I. Pettigrew and S. Ma, *Small*, 2024, **20**, 2306940.
39 S. S. Y. Chui, S. M. F. Lo, J. P. H. Charmant, A. G. Orpen and I. D. Williams, *Science*, 1999, **283**, 1148–1150.
40 A. C. Sudik, A. P. Côté and O. M. Yaghi, *Inorg. Chem.*, 2005, **44**, 2998–3000.
41 H. Li, M. Eddaoudi, M. O'Keeffe and O. M. Yaghi, *Nature*, 1999, **402**, 276–279.
42 A. Rajan, M. Sharma and N. K. Sahu, *Sci. Rep.*, 2020, **10**, 15045.
43 C. Kim, J. Lee, D. Schmucker and J. D. Fortner, *npj Clean Water*, 2020, **3**, 8.
44 D. L. Peréz, I. Puentes, G. A. M. Romero, I. M. S. Gaona, C. A. P. Vargas and R. J. Rincón, *J. Nanoparticle Res.*, 2023, **26**, 2.
45 L. Yang, K. Wang, L. Guo, X. Hu and M. Zhou, *J. Mater. Chem. B*, 2024, **12**, 2670–2690.
46 A. Domán, O. Czakkel, L. Porcar, J. Madarász, E. Geissler and K. László, *Appl. Surf. Sci.*, 2019, **480**, 138–147.
47 I. Simonsson, P. Gärdhagen, M. Andrén, P. L. Tam and Z. Abbas, *Dalton Trans.*, 2021, **50**, 4976–4985.
48 B. Chen, X. Wang, Q. Zhang, X. Xi, J. Cai, H. Qi, S. Shi, J. Wang, D. Yuan and M. Fang, *J. Mater. Chem.*, 2010, **20**, 3758–3767.